High-precision finite-size scaling analysis of the quantum-critical point of $S=1/2$ Heisenberg antiferromagnetic bilayers

Ling Wang,* K. S. D. Beach,† and Anders W. Sandvik‡
Department of Physics, Boston University, 590 Commonwealth Avenue, Boston, Massachusetts 02215, USA
(Received 28 September 2005; revised manuscript received 23 November 2005; published 27 January 2006)

We use quantum Monte Carlo (stochastic series expansion) and finite-size scaling to study the quantum critical points of two $S=1/2$ Heisenberg antiferromagnets in two dimensions: a bilayer and a Kondo-lattice-like system (incomplete bilayer), each with intraplane and interplane couplings J and $J_\perp$. We discuss the ground-state finite-size scaling properties of three different quantities—the Binder moment ratio, the spin stiffness, and the long-wavelength magnetic susceptibility—which we use to extract the critical value of the coupling ratio $g=J_\perp/J$. The individual estimates of g_c are consistent provided that subleading finite-size corrections are properly taken into account. For both models, we find that the spin stiffness has the smallest subleading finite-size corrections; in the case of the incomplete bilayer we find that the first subleading correction vanishes or is extremely small. In agreement with predictions, we find that at the critical point the Binder ratio has a universal value and the product of the spin stiffness and the long-wavelength susceptibility scales as $1/L^2$ with a universal prefactor. Our results for the critical coupling ratios are $g_c=2.5220(1)$ (full bilayer) and $g_c=1.3888(1)$ (incomplete bilayer), which represent improvements of more than an order of magnitude over the previous best estimates. For the correlation length exponent we obtain $\nu=0.7106(9)$, consistent with the expected three-dimensional Heisenberg universality class.

DOI: 10.1103/PhysRevB.73.014431 PACS number(s): 75.10.Jm, 75.10.−b, 75.40.Cx, 75.40.Mg

I. INTRODUCTION

The two-dimensional (2D) $S=1/2$ Heisenberg antiferromagnet has received considerable attention in the past two decades because of its close relation to the CuO_2 layers of the cuprate superconductors.[1] Other, even better realizations of this model system have been discovered as well.[2] The properties of the single-layer Heisenberg model have been thoroughly studied using both analytical and numerical methods, and there is very good agreement with experiments, e.g., for the temperature dependence of the spin correlation length[3,4] in La_2CuO_4 (measured using neutron scattering) and NMR relaxation rates.[5]

Mapping the lattice Heisenberg model onto a continuum field theory yields the $(2+1)$-dimensional nonlinear σ model,[3,6] the coupling constant g of which controls the transition from Néel order to quantum disorder at temperature $T=0$ (a quantum phase transition[7]). This transition is in the universality class of the finite-T transition of the 3D classical Heisenberg model.[3,8] Having an ordered ground state,[9] the 2D square-lattice $S=1/2$ Heisenberg model corresponds to $g<g_c$. Even so, there is some influence from the critical point, because a quantum phase transition is also associated with universal quantum critical scaling at finite temperature, in an extended (g,T) regime where temperature is the dominant energy scale.[10] The energy scales characterizing the ordered and disordered phases—the spin stiffness and the singlet-triplet gap, respectively—vanish continuously as $g \to g_c$, and hence the quantum critical regime fans out from the point $(g=g_c, T=0)$.

A quantum phase transition of the type described by the nonlinear σ model can be realized in the Heisenberg antiferromagnet by introducing a pattern of two (or more) different coupling strengths in a way that favors singlet formation on dimers (or larger units of an even number of spins).[3,10] This leads to an order-disorder transition at some critical coupling ratio. Models of this kind, e.g., a bilayer where dimers form across the layers,[11–13] single layers with various dimer patterns,[14,15] or a regularly depleted system where singlets form on rings of four or eight spins,[16] have been extensively studied using quantum Monte Carlo simulations in order to confirm the expected universality class and to test very detailed predictions[10] of the finite-T quantum critical behavior of various quantities. The predicted universal behavior was confirmed at low temperature.[13,15–18] The simulations also served to establish the onset of nonuniversal lattice effects at higher temperature and the nature of the crossover[10] to the low-temperature renormalized classical or quantum-disordered regimes away from the critical point.

In this paper we study the critical points of two different $S=1/2$ Heisenberg models: a symmetric bilayer and a Kondo-lattice-like system in which there are no intraplane couplings in one of the layers. We will refer to these systems as the full and incomplete bilayers, respectively; see Fig. 1. Their Hamiltonians (H_1 for the full bilayer and H_2 for the incomplete bilayer) are given by

$$H_1 = J\sum_{\langle i,j\rangle} (\mathbf{S}_{1i}\cdot\mathbf{S}_{1j} + \mathbf{S}_{2i}\cdot\mathbf{S}_{2j}) + J_\perp \sum_i \mathbf{S}_{1i}\cdot\mathbf{S}_{2i}, \qquad (1)$$

$$H_2 = J\sum_{\langle i,j\rangle} \mathbf{S}_{1i}\cdot\mathbf{S}_{1j} + J_\perp \sum_i \mathbf{S}_{1i}\cdot\mathbf{S}_{2i}. \qquad (2)$$

Here, $\mathbf{S}_{a,i}$ is a spin-1/2 operator at site i of layer a ($a=1,2$), and $\langle i,j\rangle$ denotes a pair of nearest-neighbor sites on the square lattice of $L\times L$ sites with periodic boundary conditions. Both coupling constants are antiferromagnetic ($J, J_\perp > 0$). In order to avoid any frustration we consider only even L. As the ratio $g=J_\perp/J$ is increased, there is a tendency to form interplane near-neighbor singlets, which at

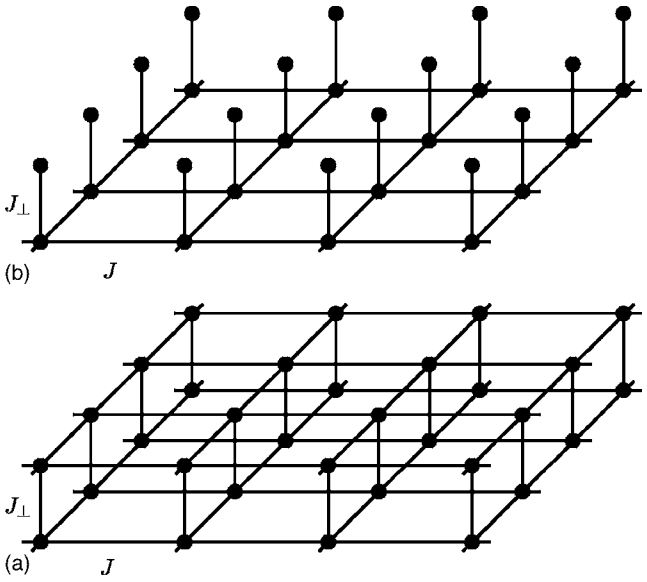

FIG. 1. The arrangement of spin interactions in the (a) full and (b) incomplete bilayers. There are two different couplings: J (intraplane) and $J_\perp$ (interplane), as indicated.

some $g=g_c$ leads to the opening of a spin gap and destruction of the long-range Néel order present for $g<g_c$ (in the limit $g\to\infty$ the ground state is a singlet product, which clearly cannot support long-range spin-spin correlations). This is the transition we investigate in detail in this paper.

Our purpose in studying these models is twofold. First, we would like to determinate the locations of the critical points to much higher accuracy than they are currently known. The best estimates to date are $g_c=2.525(2)$ (full bilayer)[17] and $g_c=1.393(8)$ (incomplete bilayer)[21] (see also Ref. 18). The statistical accuracies here are quite modest compared to results for the standard classical critical points (e.g., the 3D Heisenberg model[19,20]). It would be useful to increase the precision so that studies of various aspects of finite-T quantum criticality (e.g., interesting properties of isolated impurities in a critical host system[22–26]) could be studied numerically at low T very close to the critical point (minimizing the effects of the eventual crossover to the renormalized-classical or quantum-diosrdered regime). Second, we wish to compare several different ways of extracting the critical coupling, in order to gain additional confidence in the results and to provide guidance for studies of other quantum critical points. The reason for choosing the particular bilayer lattices of Fig. 1, over other 2D Heisenberg systems undergoing the same type of transition, is that they do not break any in-plane symmetries of the square lattice.

We have carried out finite-size scaling of low-temperature ($T\to 0$ converged) QMC results for three different quantities: the Binder cumulant ratio, the spin stiffness, and the long-wavelength (uniform) magnetic susceptibility. We use our recently proposed method for including subleading finite-size corrections.[27] Although this necessitates nonlinear fits with a relatively large number of independent parameters, we believe that this is necessary in order to minimize systematic errors. Our final results for the critical couplings are $g_c=2.5220(1)$ for the full bilayer and $g_c=1.3888(1)$ for the incomplete bilayer, i.e., the precision is improved by approximately one and two orders of magnitude, respectively, relative to the previous estimates. In addition to statistical uncertainties, the error bars here reflect estimates of the effects of remaining systematic errors, which are due to neglected higher-order subleading corrections. We have estimated these using a consistency check of universal quantities not included in the fits.

Our fitting procedure also gives the correlation-length exponent ν, but because of the multiparameter fits and the relatively modest lattices sizes (L up to 42), its precision is not quite as high (the error bars are roughly twice as large) as that of recent classical Monte Carlo simulations of the 3D Heisenberg model.[20] Nevertheless, our result $\nu=0.7106(9)$ is fully consistent with the presently most accurate value of this exponent $\nu=0.7112(5)$.[20]

We also present results for universal quantities at the critical point. The Binder moment ratio is dimensionless and independent of system size to leading order in $1/L$. We find that its value in the $g\to g_c$, $L\to\infty$ limit is consistent for each of the two different bilayer models. The spin stiffness and the long-wavelength susceptibility, on the other hand, are dimensionful quantities and are believed to scale as c/L and $1/cL$ with universal prefactors.[10] Since we have no independent estimate of c, the spin-wave velocity, we cannot test this prediction directly. We do, however, verify that the product of the spin stiffness and susceptibility scales as $1/L^2$ with a universal prefactor.

The rest of the paper is organized as follows. In Sec. II we discuss the quantities that we have calculated and their QMC [stochastic series expansion (SSE)] estimators, as well as their expected finite-size scaling forms. In Sec. III we first briefly review our approach to deal with subleading finite-size corrections and then present the results of the analysis. We give a brief summary and conclusions in Sec. IV.

II. CALCULATED OBSERVABLES AND THEIR CRITICAL SCALING PROPERTIES

We have used the SSE QMC method with operator-loop updates.[28] This approach is based on sampling diagonal matrix elements of the power series expansion of $\exp(-\beta H)$, where β is the inverse temperature. We use $L\times L\times 2$ lattices with periodic boundary conditions in the x and y directions, with even L up to 42. In order to ensure convergence of all calculated quantities to their ground-state values, we carried out simulations at inverse temperatures $\beta_n=2^n$ with integer n taken large enough so that results for β_n and β_{n-1} agree within statistical errors. Examples of the convergence are shown in Fig. 2.

A. Binder moment ratios Q_k

The magnetic moment ratios Q_k introduced by Binder[31] have the very useful property of being universal at the critical point, because all nonuniversal scale factors cancel out along with the length dependence. This follows from the finite-size scaling hypothesis for the ordered moment (here

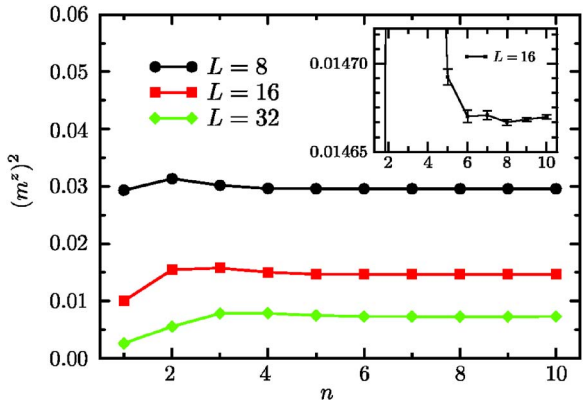

FIG. 2. (Color online) Convergence as a function of inverse temperature $\beta=2^n$ of the squared sublattice magnetization to its ground state value for three different lattice sizes. The inset shows the behavior for $L=16$ on a more detailed scale.

the staggered magnetization). The kth power of the staggered magnetization scales as

$$\langle |m|^k \rangle_L = L^{-k\beta/\nu} M_k(tL^{1/\nu}), \tag{3}$$

where L is the linear system length, β and ν are critical indices in their standard notation, and t is the reduced coupling constant, which we define here in terms of the coupling ratio g as $t=(g-g_c)/g_c$. $M_k(x)$ are the scaling functions. Consequently, the moment ratios

$$Q_k(t,L) = \frac{\langle m^{2k} \rangle_L}{\langle m^2 \rangle_L^k} \tag{4}$$

are dimensionless scaling functions. At the critical point, $Q_k(0,\infty)$ are universal constants.

We have computed the first two Binder ratios, which we define as

$$Q_1 = \frac{\langle m^2 \rangle}{\langle |m| \rangle^2} = \frac{3\langle (m^z)^2 \rangle}{2\langle |m^z| \rangle^2}, \tag{5}$$

$$Q_2 = \frac{\langle m^4 \rangle}{\langle m^2 \rangle^2} = \frac{5\langle (m^z)^4 \rangle}{3\langle (m^z)^2 \rangle^2}, \tag{6}$$

where m^z is the z component of the staggered magnetization operator

$$m^z = \frac{1}{N}\sum_{i=1}^{N} S_i^z (-1)^{x_i+y_i} = m\cos(\Theta). \tag{7}$$

Here, $N=2L^2$ is the number of lattice sites. Since the $O(3)$ spin-rotational symmetry is not broken in the simulations in the ordered phase (i.e., an average over all angles Θ is obtained) we have included the appropriate factors to compensate for the rotational averaging of m^z in Eqs. (5) and (6).

In Fig. 3 we show the ratio Q_2 for both bilayer systems as a function of g for lattices of different linear length L. One can clearly see the curve crossings, indicating a quantum critical point, but it is apparent that there are sizable corrections to their location. We will analyze these crossing-point shifts in Sec. III.

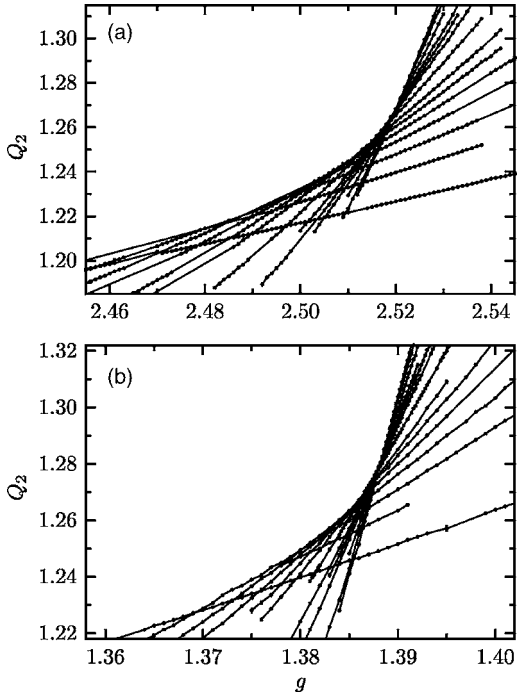

FIG. 3. The Binder ratio Q_2 is plotted as a function of the coupling ratio for the (a) full and (b) incomplete bilayers. Results for even L from 8 to 42 are shown (all except for $L=22,26,34,38$). The slope of the curves increases with L.

Note that Q_2 at the crossing point is approximately the same for both models, in accord with an expected universal value as $L\to\infty$. Simulations done on 3D classical Heisenberg models[19,20,29] gave a universal value in the range 1.35-1.40, i.e., substantially larger than what we see in Fig. 3 (clearly these values have not yet completely converged to their infinite-size Q_2, and the trend is for the crossing value to increase with L, but we will show that they converge to $Q_2 \approx 1.29$). This disagreement with the classical value is easily accounted for by considering the way the sublattice magnetization is defined and computed in a quantum system: Although the 2D system formally is mapped onto a 3D classical model, $\langle |m^z|^k \rangle$ is an equal-time expectation value, which in the simulations is averaged over the third (imaginary time) direction. This corresponds directly to taking expectation values over individual layers in a 3D classical model. We are not aware of any such calculation and hence cannot compare directly with the corresponding classical universal value. Nevertheless, as we will show in greater detail in Sec. III, the crossing Q_2 values for both our systems are fully consistent with each other and hence support universality.

B. Spin stiffness ρ_s

In continuum field theory language, a stiffness ρ is defined in terms of the increase in free-energy density f as a boundary-condition twist Φ is imposed on the order-parameter field θ:

$$\delta f_s(t,L) = \frac{1}{2}\rho(\nabla\theta)^2 = \frac{1}{2}\rho(\Phi/L)^2. \tag{8}$$

The prefactor is the stiffness constant

$$\rho = L^2 \frac{\partial^2 f_s}{\partial \Phi^2}. \tag{9}$$

At a quantum critical point, it should scale as[30]

$$\rho \sim L^{2-d-z}, \tag{10}$$

where d is the dimensionality and z is the dynamic critical exponent.

For the Heisenberg model, the spin stiffness ρ_s is determined by imposing a twist directly in the Hamiltonian, modifying the spin-spin interactions in one of the lattice directions $\mathbf{S}_i \cdot \mathbf{S}_j \rightarrow \mathbf{S}_i \cdot \mathbf{R}(\Phi/L)\mathbf{S}_j$, where $\mathbf{R}$ rotates the spin operator about an appropriately chosen axis.[32] In SSE simulations, like in path integrals,[33] the stiffness is directly obtained without explicitly imposing a twist, as the second derivative of the energy with respect to the twist at $\Phi=0$. This leads to an estimator in terms of winding number fluctuations[32]

$$\rho_s = \frac{3}{4}\langle w_x^2 + w_y^2 \rangle / \beta, \tag{11}$$

where the winding numbers are

$$w_\alpha = (N_\alpha^+ - N_\alpha^-)/L \quad (\alpha = x,y). \tag{12}$$

Here N_α^+ (N_α^-) is the number of operators $S_i^+ S_j^-$ ($S_i^- S_j^+$) in the sampled terms of the power series expansion, with i,j two nearest-neighbor sites oriented along the lattice α (x or y) axis. The definition (11) corresponds to the stiffness per unit cell of the bilayer models.

In the case of the bilayer models we have $d=2$ and expect $z=1$, and hence the scaling (10) becomes $\rho_s \sim L^{-1}$. The quantity $\rho_s L$ should thus be size independent at the critical point, and also in this case one can expect curves for different L to cross each other. Such crossings have previously been used to approximately locate the critical point of the full bilayer.[32] In two dimensions, ρL should be a universal number times the spin-wave velocity.[10]

Figure 4 shows our SSE results for $\rho_s L$ versus g for different lattice sizes. Again, one can see that the crossing points move as L is increased, but, interestingly, much less so for the incomplete than the complete bilayer. We will quantify these differences in the finite-size corrections in Sec. III.

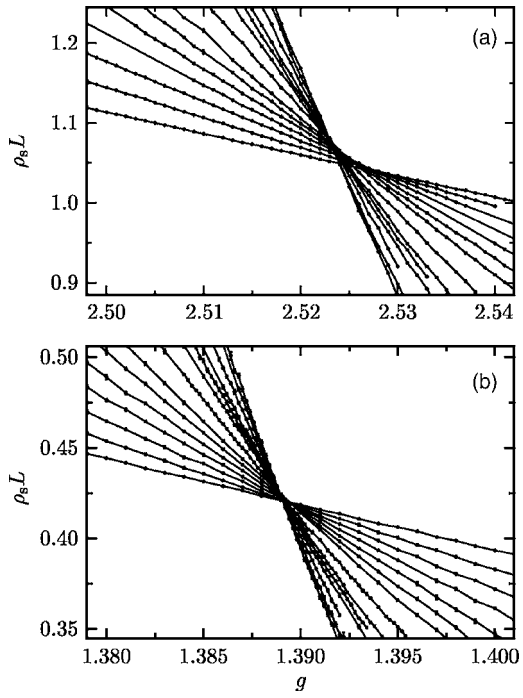

FIG. 4. The spin stiffness multiplied by the system length L versus coupling ratio for the (a) full and (b) incomplete bilayers. The system sizes are the same as in Fig. 3. The slope of the curves increases with L.

C. Uniform susceptibility $\chi(q \rightarrow 0)$

The temperature dependence of the uniform magnetic susceptibility

$$\chi_u = \frac{\beta}{N}\langle (M^z)^2 \rangle, \quad M^z = \sum_{i=1}^{N} S_i^z, \tag{13}$$

is an often-used indicator of quantum criticality. Exactly at $g=g_c$, its general asymptotic scaling form is[10]

$$\chi_u(T) \sim T^{d/z-1}. \tag{14}$$

This has been numerically confirmed at low T in previous QMC simulations[13,17] and series expansions[34] of the bilayer and other critical Heisenberg systems.[35] Here we will consider the corresponding finite-size scaling behavior, which we obtain by substituting the finite-T quantum critical correlation length $\xi \sim T^{-1/z}$,[3,10] in the temperature dependence (14) and then substituting L for ξ, giving $\chi_u \sim L^{z-d}$. However, we apparently have a problem here since for a finite system χ_u vanishes as $T \rightarrow 0$, due to the conserved magnetization M^z and the singlet ground state. In order to carry out finite-size scaling, we therefore consider the long-wavelength limit of the wave-vector-dependent susceptibility $\chi(\mathbf{q})$, which we obtain in practice by taking $q=2\pi/L$. Thus we will test the finite-size scaling form

$$\chi(q \rightarrow 0) = \chi(2\pi/L) \sim L^{z-d}. \tag{15}$$

The static spin-spin susceptibility in real space is given by the Kubo integral

$$\chi(k,l) = \int_0^\beta d\tau \langle S_k^z(\tau) S_l^z(0) \rangle, \tag{16}$$

which in SSE simulations is obtained in terms of spins in the states propagated by the sampled operator sequences[32]

$$\chi(k,l) = \left\langle \frac{\beta}{n(n+1)} \left(\sum_{p=0}^{n-1} S_k^z[p] \right) \left(\sum_{p=0}^{n-1} S_l^z[p] \right) + \frac{\beta}{(n+1)^2} \left(\sum_{p=0}^{n} S_k^z[p] S_l^z[p] \right) \right\rangle. \tag{17}$$

n is the number of Hamiltonian operators in the sampled sequences and the index p refers to the state obtained after p operators have acted. The Fourier transform that we are interested in is

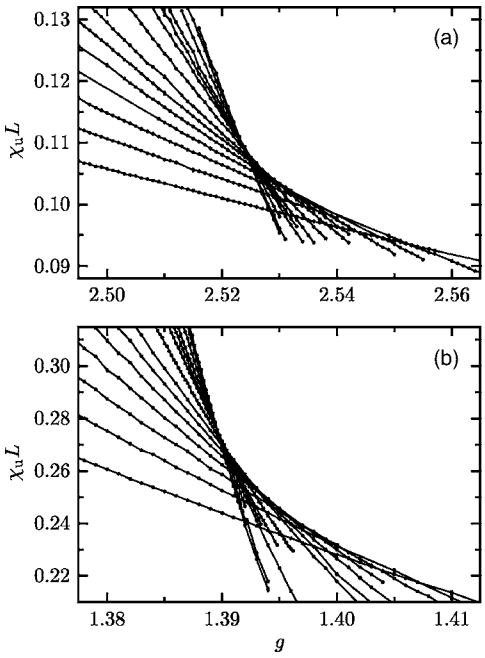

FIG. 5. The long-wavelength susceptibility multiplied by the system length versus the coupling ratio for the (a) full bilayer and (b) incomplete bilayer. The system sizes are those listed in Fig. 3. The slope of the curves again increases with L.

$$\chi(\mathbf{q}) = \frac{1}{N}\sum_{k,l} e^{i\mathbf{q}\cdot(\mathbf{r}_k-\mathbf{r}_l)}\chi(k,l), \tag{18}$$

and since our models are symmetric with respect to a 90° rotation, we take the long-wavelength susceptibility as

$$\chi_u = \chi(q\to 0) = \frac{1}{2}\left[\chi\left(\frac{2\pi}{L},0,0\right) + \chi\left(0,\frac{2\pi}{L},0\right)\right]. \tag{19}$$

We again consider the form leading to curve crossings at the critical point, i.e., we plot $\chi_u L$, which should be size independent at g_c. Figure 5 shows the data that we will anayze more carefully in the next section. Again we observe crossing points, which shift significantly with L.

III. DATA ANALYSIS

We first discuss here a rough determination of the critical coupling ratios of the two models, studying the asymptotic behavior of the crossing points discussed above. This will also serve as a first confirmation of mutual consistency of the leading scaling forms for the three different quantities under consideration. We then analyze the results in greater detail using a finite-size scaling hypothesis including subleading corrections.

A. Critical coupling from crossing points

We use the data presented in the previous section to extract the intersection points of fixed-L curves for system sizes L and $2L$ (other size ratios give similar results). Our simulations have been performed on a rather dense grid of g values, and we can therefore reliably obtain the intersection points

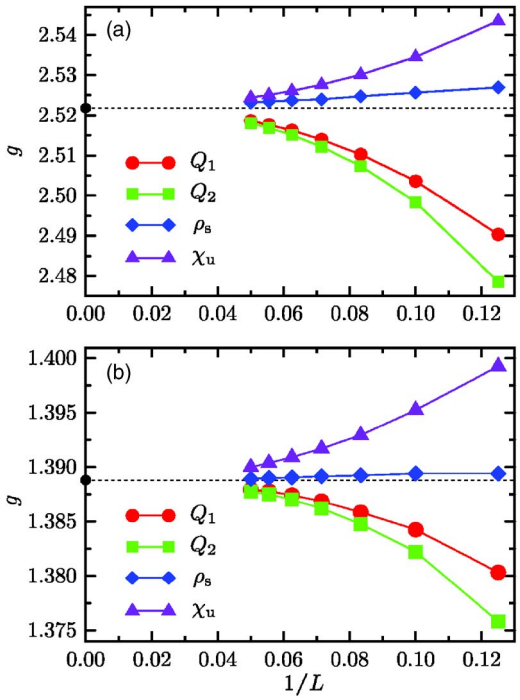

FIG. 6. (Color online) Convergence versus the inverse lattice size of intersection points of curves for L and $2L$, for the (a) full and (b) incomplete bilayers. The error bars are are much smaller than the symbols. The circles at $1/L=0$ indicate the critical couplings from the careful finite-size scaling analysis carried out in Sec. III B.

using fits of straight lines or second-order polynomials to interpolate between the data points. In Fig. 6 we plot the results versus the inverse system size. For both models, the crossing points drift toward a common critical coupling in the $L\to\infty$ limit, thus confirming the scaling laws discussed in the previous section.

For both models, especially the incomplete bilayer, the spin stiffness crossing point exhibits the most rapid convergence (i.e., the weakest subleading corrections). It and the susceptibility converge from above, while the Binder ratios converge from below. We can hence bracket g_c using these results. However, a much more precise bracketing can be obtained from the spin stiffness curves alone, noting that they become very flat as L grows. With the curvature decreasing with increasing L, a straight-line extrapolation using a few large-L points (we use four) should give a lower bound for g_c, while the crossing point for the largest L should be an upper bound. The critical couplings extracted this way are $g_c \in (2.5205, 2.5232)$ and $g_c \in (1.38870, 1.38895)$ for the full and incomplete bilayers, respectively. These values are fully consistent with the best previous estimates, discussed in Sec. I but the precision is significantly higher. The more rigorous data analysis discussed below will further improve on the accuracy.

Naively, one might expect that the asymptotic approach of the crossing points to the critical coupling should be given by the correlation-length exponent ν, as $g_{\rm cross} = g_c + aL^{-1/\nu}$, as is the case for fixed-size estimates of the critical coupling (or the critical temperature), such as the location of the maximum of the order-parameter susceptibility or the specific

heat (in the case of finite-T transitions). However, a crossing point cannot be regarded as a conventional fixed-L definition of g_c, since two system sizes are involved and there can be cancelation of the leading behavior defined in terms of the individual lattices. Thus, we would in general expect the crossing points to converge faster than $L^{-1/\nu}$. Binder has discussed the corrections to the cumulant crossing-points,[31] and in a recent article[27] we have presented a different way of analyzing crossing points in general (i.e., not only for Binder ratios but also for other quantities that are size independent at g_c) which takes subleading finite-size corrections into account explicitly. There we also showed some results for the spin stiffness crossings of the full bilayer model. Here we will not analyze the crossing points in any greater detail, but instead consider the scaling of the full fixed-L curves shown in the figures of Sec. II. Such "data collapse" makes better use of the full range of simulation results and can also be carried out with subleading corrections taken into account.[27]

B. Finite-size scaling with subleading corrections

The scaling ansatz typically used to analyze finite-size data $A(t,L)$ for a quantity A at reduced coupling $t=(g-g_c)/g_c$ on a lattice of length L is

$$A(t,L) = L^{\kappa/\nu} f_A(tL^{1/\nu}), \tag{20}$$

where κ is a critical exponent which depends on the quantity A, i.e., $A(t,L=\infty)\sim t^{-\kappa}$. This form can be used to collapse data in a neighborhood of $t=0$, by graphing $A(t,L)L^{-\kappa/\nu}$ versus $tL^{1/\nu}$, adjusting g_c, κ, and ν to obtain the tightest collapse of the data onto a single curve.

In Ref. 27 we started from renormalization group theory and derived an extension to Eq. (20) that includes both "shift" and "renormalization" corrections

$$A(t,L) = L^{\kappa/\nu}(1+cL^{-\omega}) g_A(tL^{1/\nu} + dL^{-\phi/\nu}). \tag{21}$$

Here, ϕ is the subleading irrelevant RG eigenvalue, which causes a shift in the critical coupling, and ω is an effective exponent that accounts for corrections due to the inhomogeneous part of the free energy and nonlinearity of the scaling fields. The constants c and d are nonuniversal and should be regarded as fitting parameters along with the leading and subleading exponents. From Eq. (21), we see that we can now achieve data collapse by plotting $A(t,L)L^{-\kappa/\nu}/(1+cL^{-\omega})$ versus $x=tL^{1/\nu}+dL^{-\phi/\nu}$ for different sizes L.

To carry out this type of analysis in practice, we note that the scaling function $g_A(x)$ is well behaved and can be Taylor expanded close to the critical point

$$g_A(x) = A(t,L)L^{-\kappa/\nu}/(1+cL^{-\omega}) = q_0 + q_1 x + q_2 x^2 + q_3 x^3 + q_4 x^4 + \cdots . \tag{22}$$

For the Heisenberg bilayers, the critical indices κ and ν are expected to be those of the 3D classical Heisenberg universality class. In the case of the ratios we are considering, κ/ν are known integers which we hence do not have to adjust. The current best estimate for the correlation length exponent is $\nu=0.7112(5)$,[20] but in our analysis we keep it as a free parameter, along with g_c, the subleading exponents ω and ϕ,

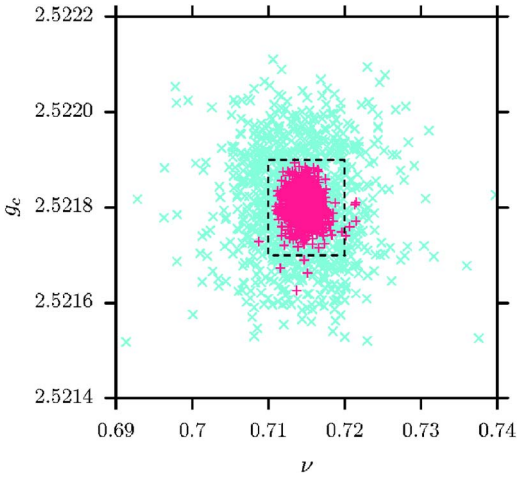

FIG. 7. (Color online) The blue crosses (×) show the input points of the optimization procedure. The red plusses (+) show the output. The dashed black line indicates the magnified region correspondig to the bottom-right plot in Fig. 8.

the constants c and d, and the parameters of the polynomial in Eq. (22). This amounts to a large number of fitting parameters, but it should be noted that the polynomial expansion of the scaling function is essentially just an interpolation of the data and hence is highly constrained; the freedom in the coefficients q_i do not add significant freedom to the other paramers of the fit (we use a quartic polynomial). Moreover, the number of fitting parameters is dwarfed by the number of data points to be fit (hundreds or thousands).

Nonlinear curve fitting has well-known problems associated with the convergence of the parameters to the globally optimal fit. In our work we already know rather accurate estimates for ν and g_c, and at the first stage of the fits we used those values as initial conditions. Once we obtained rough estimates for c,ω,d,ϕ, we used the following procedure: Performing bootstrap sampling of the raw data, we carried out a large number (typically around 1000) of fits with initial conditions for all the parameters taken at random from inside a "box" in parameter space. This box is determined such that the fits converge well, but that the variation in starting points is significantly larger than the final spread of the resulting parameters. We then use the spread among the bootstrap samples to calculate statistical errors. This procedure is illustrated in Figs. 7 and 8.

The scaling formula (21) is strictly valid only for large lattices and a small range of couplings in the vicinity of g_c [although the range of validity should be larger than with the leading-order form (20)]. The parameters obtained show some dependence on the range of data included. In order to eliminate as much as possible potential remaining effects of further subleading corrections that are not captured by our approach, we chose to use a rather narrow window in the scaled coupling $x=(g-g_c)L^{1/\nu}/g_c+dL^{-\phi/\nu}$, so that there is no longer any statistically detectable dependence on the size of the window. Our final results are based on $x\in[-0.25,0.25]$. There are also other subtle issues in the fitting procedure, e.g., for a given range of x, different number of data points are available for the different lattice sizes, typically leading

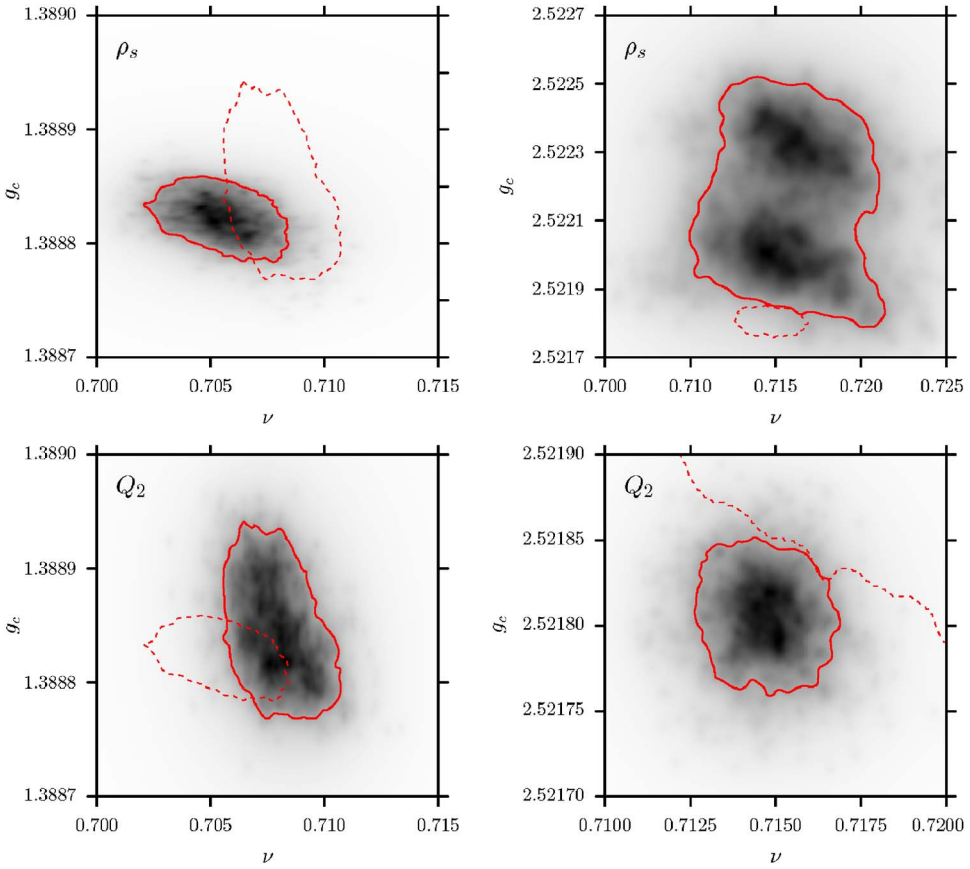

FIG. 8. (Color online) The number density of bootstrapped (ν, g_c) solutions is plotted for Q_2 and ρ_s in greyscale. The left panel shows the incomplete bilayer and the right panel the complete bilayer. The solid red lines show the contour at 1/3 the maximum density (this would correspond to 2/3 of the weight under a gaussian distribution). In the top right panel, note a two-peak structure which sometimes appears in the nonlinear fits. The dotted lines are guides to the eye. They show the Q_2 contour on the ρ_s plot and vice versa.

to relatively smaller statistical weight for the larger sizes than the smaller sizes. We therefore made sure to include only system sizes sufficiently large for the extracted parameters not to change appreciably when systematically excluding more of the smaller lattices. We kept only $L \geqslant 8$ for the results we report here.

We found both the Binder ratio and the spin stiffness to be well behaved in the fitting procedures. The resulting collapsed data for these quantities, i.e., their scaling functions $g_A(x)$ in Eq. (23), are shown in Figs. 9 and 10. We do not discuss results for Q_1 here as it behaves similarly to Q_2 and is statistically strongly correlated to it. The long-wavelength susceptibility also exhibits data collapse, however, with substantially larger fluctuations than ρ_s and Q_2 (the prefactor d appears to be rather large and difficult to determine accurately, and thus it is difficult to fix the data window $x \in [x_{\min}, x_{\max}]$ in a meaningful way). We have therefore focused on ρ_s and Q_2 for the final high-precision statistical analysis.

For the subleading exponents ω and ϕ we obtain the following values: For the full bilayer, $\omega = 1.14(3)$, $\phi = 0.8(2)$ in the Q_2 scaling and $\omega = 1.0(3)$, $\phi = 1.2(2)$ in the ρ_s scaling. For the incomplete bilayer, $\omega = 1.0(4)$, $\phi = 1.3(2)$ in Q_2 and $\omega = 1.9(2)$, $\phi = 1.8(2)$ in ρ_s. All these subleading exponents should be interpreted as effective ones, as they are to some extent affected by the higher-order corrections that we have neglected. In any case, we note that all subleading exponents, with the notable exception of both ω and ϕ obtained from ρ_s of the incomplete bilayer, are close to 1. The fact that ω and ϕ obtained from ρ_s of the incomplete bilayer are close to 2 suggests that in this case the leading corrections vanish or are very small, and the extracted exponents instead reflect predominantly the corrections of the next higher order.

We have also performed fits of the combined quantity $\rho_s \chi_u$, which is better behaved than χ_u alone. This quantity is not statistically independent of ρ_s, and we do not use it in our final determination of g_c and ν (although doing so has almost no effect on the final results). Rather, we focus on the value of its scaling function at the origin in order to test for universality at the critical point. As a check, we compare this with the product of the values obtained from the individual ρ_s and χ_u fits and find that they are consistent.

The final parameters and their statistical errors were determined from the bootstrap samples. The distributions are illustrated by density plots in Fig. 8. We list the values for g_c, ν, and the value of the respective quantities at the critical point $q_0 = Q_2(g_c), \rho_s(g_c)L, \ldots$ in Table I. The critical couplings are consistent among all the fits, and the correlation length exponent is marginally consistent (within 2-3 standard deviations).

As seen in the table, the highest relative precision of g_c is obtained using Q_2 for the full bilayer and ρ_s for the incomplete bilayer. The latter can probably be traced to very small subleading corrections, as is evident already in Fig. 4. For the full bilayer ρ_s also has smaller subleading corrections than Q_2, but still we obtain a higher precision in g_c using Q_2. What this may tell us is that small subleading corrections are not necessarily advantageous—that what matters is how well those corrections are described by the finite-size scaling forms used. Alternatively, it may be a sign that our bootstrap procedure is somehow underestimating the statistical uncer-

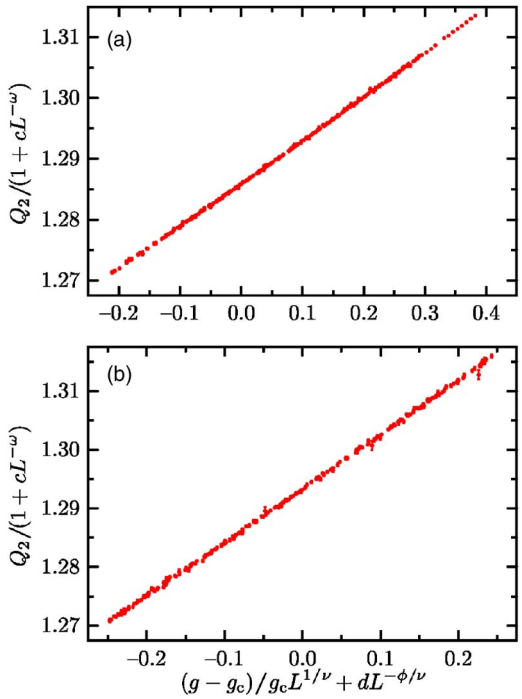

FIG. 9. (Color online) Data collapse of the Binder ratio for the (a) full and (b) incomplete bilayer. The values of g_c and ν obtained are listed in Table I.

tainty in the nonlinear fitting of the Q_2 data. Indeed, looking at Table I, the result $g_c=2.52180(3)$ stands out as a little low (although statistically consistent) in comparison with the other estimates. In the complete bilayer (right-hand) plots of

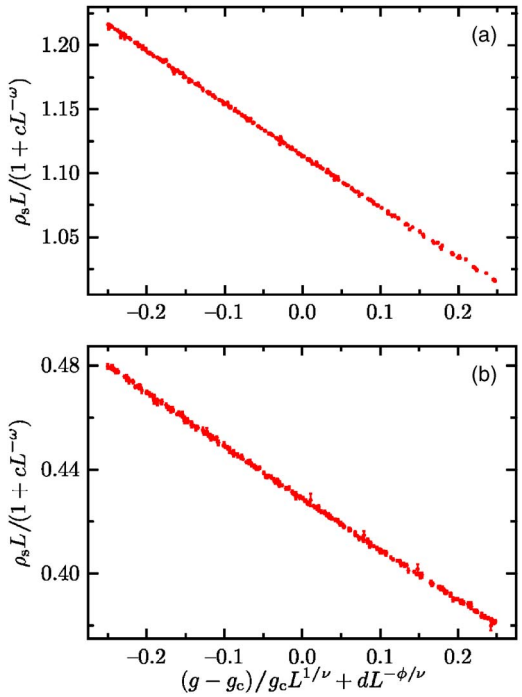

FIG. 10. (Color online) Data collapse of the spin stiffness ratio for the (a) full and (b) incomplete bilayer. The values of g_c and ν obtained are listed in Table I.

TABLE I. Bootstrap averages and error bars for the parameters g_c, ν, q_0 (the values of the respective quantities at g_c). The top group of values are for the incomplete bilayer, and the bottom group for complete bilayer. The indicated error bars correspond to one standard deviation of the probability distributions obtained in the bootstrap analysis, as explained in the text.

	g_c	ν	q_0
Q_2	1.38885(5)	0.708(2)	1.293(3)
ρ_sL	1.38882(2)	0.705(2)	0.434(3)
χ_uL	1.388(1)	0.7(1)	0.28(2)
$\rho_s\chi_uL^2$	1.3888(1)	0.714(5)	0.11(2)[a]
Q_2	2.52180(3)	0.715(2)	1.2858(3)
ρ_sL	2.5221(2)	0.714(5)	1.13(3)
χ_uL	2.521(1)	0.7(1)	0.12(2)
$\rho_s\chi_uL^2$	2.5220(2)	0.706(4)	0.132(8)[b]

[a]Compare to the product of the individual ρ_sL and χ_uL estimates $0.434(3)\times0.28(2)=0.12(1)$.
[b]As in[a] for $1.13(3)\times0.12(2)=0.14(3)$.

Fig. 8, the Q_2 distribution appears as a small satellite adjacent to the ρ_s distribution, which is quite unlike the situation in the incomplete bilayer, where there is considerable overlap between the comparably sized Q_2 and ρ_s distributions. We will argue below that the statistical uncertainty is estimated correctly but that there are remaining systematic errors due to neglected higher-order finite-size corrections. The errors can be as large or larger than the statistical ones.

Let us suppose that the magnitude of the statistical uncertainties has been correctly determined. Then the best estimates of the critical couplings are just the statistically weighted averages of the Q_2- and ρ_s-extracted values listed in Table I: $g_c=2.52181(3)$ and 1.38882(2) for the full and incomplete bilayer, respectively. If the uncertainties in the complete bilayer Q_2 fit are underestimated, then a better estimate of the critical coupling is $g_c=2.5220(1)$, which can be arrived at either by averaging the ρ_s and χ_u estimates, or by averaging those of Q_2, ρ_s, and χ_u under the assumption that the g_c error bar for Q_2 is of the same order of magnitude as for ρ_s.

In Fig. 11, we plot the (potentially) universal quantities Q_2 and $\rho_s\chi_uL^2$, evaluted at the highest-precision estimates of the critical points [$g_c=2.52181(3)$ and 1.38882(2)] by interpolating between measured data points, as a function of inverse system size. Even making the most naive extrapolation to $L=\infty$, it is clear that these quantities tend to values that differ between the two bilayer models by no more than 1% for $Q_2(g_c)$ and 10% for $\rho_s(g_c)$. It is unlikely that two wholly independent quantities would just happen to exhibit such a coincidence. Hence we do not take the small deviations as an indication of a potentially different universality class in the incomplete bilayer (due to incomplete cancelation of Berry phases[3,8,10,36]) when the layer-exchange symmetry is not present. More likely is that these quantities indeed are universal and that the two models are in the same universality class. In that case, it is clear from Fig. 11 that what discrepancies do exist can be substantially reduced by using a critical coupling in the complete bilayer that is closer to 2.5220

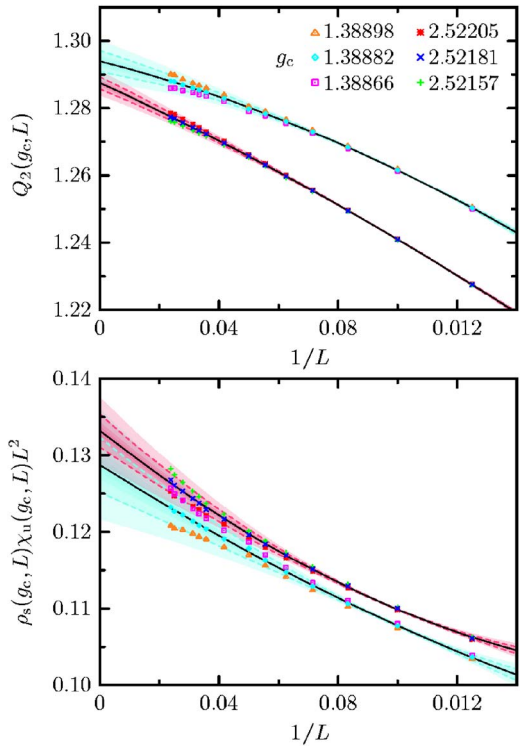

FIG. 11. (Color online) The Binder ratio (top panel) and the product of the spin stiffness and the long-wavelength susceptibility (bottom panel) are plotted as a function of inverse system size for various possible values of the critical couplings. The data points represent interpolations to the hypothetical g_c values. The solid lines and corresponding cones of graduated shading illustrate fits of the data for the most precise overall estimates $g_c=1.38882(2)$, $g_c=2.52181(3)$, and the fits at deviations of 2, 4, 8, and 16 error bars. Note that the scaling is not expected to be strictly $1/L$, and all lines should be regarded as suggestive.

than 2.52181. Making similar allowances in the incomplete bilayer, we should acknowledge that the discrepancy can also be reduced by taking a value lower than 1.38882.

Thus, it appears that we must conclude that the nonlinear fits that we have carried out above in some cases can deliver too optimistic error estimates. We do not believe that this is due to some fundamental problem with the fitting procedures or our ways of analyzing the data, but rather is a consequence of the fact that subleading corrections of higher order than those that we have included here certainly are present. The neglect of these corrections are compensated for in the fits by slight shifts of the critical point (as well as in the exponents, but since their statistical errors are much larger such shifts are comparably small and probably of no significance). Thus, there are systematic errors beyond the purely statistical errors quoted in Table I, the magnitudes of which are in general difficult to estimate. A self-consistency check using universal quantities of two different models, which we have carried out above, allows us to estimate the size of these errors. We conclude that the systematic error is large relative to the statistical error in the case of the scaling of Q_2 of the full bilayer, and potentially of the same order as the statistical errors for the other quantities. Using conservative error estimates, our final result for the critical couplings are then $g_c=2.5220(1)$ (full bilayer) and $g_c=1.3888(1)$ (incomplete bilayer). Small shifts in the critical points, of the order of our estimated errors, do not affect significantly the values of the exponents.

For the correlation length, a weighted average of the four results from ρ_s and Q_2 listed in Table I gives $\nu=0.7106(9)$. Taking a statistical average of the four individual results for ν is motivated here (as in the case of the critical point averages) in spite of the fact that they are obtained in only two different simulations. This is because the winding numbers (giving ρ_s) and the sublattice magnetization (giving Q_2) are very weakly correlated in the simulations. For the same reason, we do not include the results from $\rho_s\chi_u L^2$ in the averages, as they are quite strongly correlated to those from ρ_s alone.

IV. SUMMARY AND CONCLUSIONS

We have carried out finite-size scaling analyses of high-precision stochastic series expansion QMC data for two $S=1/2$ Heisenberg bilayer models. Using three different quantities, the Binder order parameter moment ratio, the spin stiffness, and the long-wavelength magnetic susceptibility, we have obtained very accurate estimates for the critical couplings. We have stressed the importance of including subleading corrections in the finite-size scaling analysis. All the quantities considered then give mutually consistent results for the critical couplings as well as for the correlation-length exponent ν. We have assumed that the dynamic exponent $z=1$, and all our results are completely consistent with this expectation.[3]

The inclusion of two different subleading corrections in the data fits implies larger statistical fluctuations compared to an analysis neglecting subleading corrections or taking them into account less completely than we have done here. In spite of the large freedom of the fits with several exponents, we noted a marginal inconsistency in the values of two universal numbers—the Binder ratio and the precator of the $1/L^2$ scaling of the spin stiffness times the long-wavelength susceptibility—calculated for the two models. We have shown that these inconsistencies can be explained by small shifts of the critical couplings, which are most likely due to neglected higher-order finite-size corrections. We would like to point out that such effects are not entirely surprising, because the system sizes we have studied, L up to 42, are rather modest (compared to lattice sizes commonly used in classical Monte Carlo studies) and the numerical precision of our raw data is high. By investigating the effects of shifting the critical coupling by a small amount we were able to estimate the systematic errors due to the higher-order corrections. Our final estimates for the critical couplings are $g_c=2.5220(1)$ and 1.3888(1) for the full and incomplete bilayers, respectively.

Because of the consistency checks—analyzing two universal quantities that were not included in the actual fitting procedures—we are confident that our reported error bars reflect both statistical and potential systematic errors well. We also note that the different quantities we have considered correspond to averaging functions of very different proper-

ties of the configurations generated in the simulations—the staggered magnetization in the case of the Binder ratio, the winding number in the case of the spin stiffness, and the long-wavelength magnetization in the case of the susceptibility. The consistency among all the results obtained also contribute to our confidence in the procedures.

Knowledge of the critical couplings to this level of accuracy should be useful for studies of various aspects of quantum criticality at low temperature in these systems, as one can avoid, to a higher degree than previously, effects from the eventual crossover to renormalized classical or quantum-disordered behavior as deviations from g_c become relevant as $T \to 0$.

For the correlation length exponent we obtain $\nu = 0.7106(9)$, which is consistent within error bars with the currently most accurate estimate of the 3D classical Heisenberg exponent $\nu = 0.7112(5)$ obtained from classical 3D Heisenberg simulations in Ref. 20. Although we have not quite reached the accuracy for ν obtained in the most recent classical simulations[20] (although our final error bar is actually only approximately twice as large), the precision is still sufficiently high to further increase the confidence in the belief that the universality class of the transition is that of the 3D classical Heisenberg model. The previously best (to our knowledge) determination of ν for the transition in a 2D Heisenberg system is 0.70(1).[15] The very close agreement of the universal Binder ratio at g_c also speaks in favor of the same universality class for both lattices. As further evidence, we note that the combination $\rho_s \chi_u L^2$ also appears to take a universal value, as predicted.[10] While the agreement in this case is somewhat less impressive (with uncertainties more than an order of magnitude larger), the consistency of the values taken directly from $\rho_s \chi_u L^2$ and those derived from a combination of the individual $\rho_s L$ and $\chi_u L$ fits (see Table I) lends added confidence.

ACKNOWLEDGMENTS

The authors would like to thank Subir Sachdev for helpful discussions. This work was supported by the NSF under Grant No. DMR-0513930.

*Electronic address: lingwang@buphy.bu.edu
†Electronic address: ksdb@bu.edu
‡Electronic address: sandvik@bu.edu

[1] E. Manousakis, Rev. Mod. Phys. **63**, 1 (1991).
[2] H. M. Rønnow, D.F. McMorrow, R. Coldea, A. Harrison, I. D. Youngson, T. G. Perring, G. Aeppli, O. Syljuåsen, K. Lefmann, and C. Rischel, Phys. Rev. Lett. **87**, 037202 (2001).
[3] S. Chakravarty, B. I. Halperin, and D. R. Nelson, Phys. Rev. Lett. **60**, 1057 (1988).
[4] J.-K. Kim and M. Troyer, Phys. Rev. Lett. **80**, 2705 (1998).
[5] A. W. Sandvik and D. J. Scalapino, Phys. Rev. B **51**, 9403 (1995).
[6] F. D. M. Haldane, Phys. Rev. Lett. **50**, 1153 (1983).
[7] S. Sachdev, *Quantum Phase Transitions* (Cambridge University Press, Cambridge, 1999).
[8] F. D. M. Haldane, Phys. Rev. Lett. **61**, 1029 (1988).
[9] J. D. Reger and A. P. Young, Phys. Rev. B **37**, 5493 (1988).
[10] A. V. Chubukov, S. Sachdev, and J. Ye, Phys. Rev. B **49**, 11 919 (1994).
[11] K. Hida, J. Phys. Soc. Jpn. **59**, 2230 (1990); K. Hida, *ibid.* **61**, 1013 (1992).
[12] A. J. Millis and H. Monien, Phys. Rev. Lett. **70**, 2810 (1993).
[13] A. W. Sandvik and D. J. Scalapino, Phys. Rev. Lett. **72**, 2777 (1994).
[14] R. R. P. Singh, M. P. Gelfand, and D. A. Huse, Phys. Rev. Lett. **61**, 2484 (1988).
[15] M. Matsumoto, C. Yasuda, S. Todo, and H. Takayama, Phys. Rev. B **65**, 014407 (2001).
[16] M. Troyer, H. Kontani, and K. Ueda, Phys. Rev. Lett. **76**, 3822 (1996).
[17] P. V. Shevchenko, A. W. Sandvik, and O. P. Sushkov, Phys. Rev. B **61**, 3475 (2000).
[18] W. Brenig, cond-mat/0502489 (unpublished).
[19] C. Holm and W. Janke, Phys. Rev. B **48**, 936 (1993).
[20] M. Campostrini, M. Hasenbusch, A. Pelissetto, P. Rossi, and E. Vicari, Phys. Rev. B **65**, 144520 (2002).
[21] V. N. Kotov, O. Sushkov, Zheng Weihong, and J. Oitmaa, Phys. Rev. Lett. **80**, 5790 (1998).
[22] S. Sachdev, C. Buragohain, and M. Vojta, Science **286**, 2479 (1999).
[23] M. Troyer, Prog. Theor. Phys. Suppl. **145**, 326 (2002).
[24] S. Sachdev and M. Vojta, Phys. Rev. B **68**, 064419 (2003).
[25] O. P. Sushkov, Phys. Rev. B **68**, 094426 (2003).
[26] K. H. Höglund and A. W. Sandvik (unpublished).
[27] K. S. D. Beach, L. Wang, and A. W. Sandvik, cond-mat/0505194 (unpublished).
[28] A. W. Sandvik, Phys. Rev. B **59**, R14157 (1999).
[29] A. A. Caparica, A. Bunker, and D. P. Landau, Phys. Rev. B **62**, 9458 (2000).
[30] M. P. A. Fisher, P. B. Weichman, G. Grinstein, and D. S. Fisher, Phys. Rev. B **40**, 546 (1989).
[31] K. Binder, Phys. Rev. Lett. **47**, 693 (1981); Z. Phys. B: Condens. Matter **43**, 119 (1981).
[32] A. W. Sandvik, Phys. Rev. B **56**, 11 678 (1997).
[33] E. L. Pollock and D. M. Ceperley, Phys. Rev. B **36**, 8343 (1987).
[34] N. Elstner and R. R. P. Singh, Phys. Rev. B **57**, 7740 (1998).
[35] M. Troyer, M. E. Zhitomirsky, and K. Ueda, Phys. Rev. B **55**, R6117 (1997).
[36] M. Troyer, M. Imada, and K. Ueda, J. Phys. Soc. Jpn. **66**, 2957 (1997).